Ocean Sci. Discuss., 9, 2039–2080, 2012
www.ocean-sci-discuss.net/9/2039/2012/
doi:10.5194/osd-9-2039-2012

Ocean Science
Discussions

Modeling long-term changes of the Black Sea ecosystem characteristics

V. L. Dorofeyev[1], T. Oguz[2], L. I. Sukhikh[1], V. V. Knysh[1], A. I. Kubryakov[1], and G. K. Korotaev[1]

[1]Marine Hydrophysical Institute National Academy of Sciences, Sevastopol, Ukraine
[2]Institute of Marine Sciences Middle East Technical University, Erdemli, Turkey

Received: 28 February 2012 – Accepted: 17 April 2012 – Published: 16 May 2012

Correspondence to: V. L. Dorofeyev (dorofeyev_viktor@mail.ru)

Published by Copernicus Publications on behalf of the European Geosciences Union.

Abstract

A three dimensional coupled physical-biological model is provided for the Black Sea to investigate its long-term changes under the synergistic impacts of eutrophication, climatic changes and population outbreak of the gelatinous invader *Mnemiopsis leidyi*. The model circulation field is simulated using the high frequency ERA40 atmospheric forcing as well as assimilation of the available hydrographic and altimeter sea level anomaly data for the 30 yr period of 1971–2001. The circulation dynamics are shown to resolve well the different temporal and spatial scales from mesoscale to sub-basin scale and from seasonal peaks to decadal scale trend-like changes. The biogeochemical model includes the main vertical biological and chemical interactions and processes up to the anoxic interface zone. Its food web structure is represented by two phytoplankton and zooplankton size groups, bacterioplankton, gelatinous carnivores *Mnemiopsis* and *Aurelia*, opportunistic species *Noctiluca scientillans*. The nitrogen cycling is accommodated by the particulate and dissolved organic nitrogen compartments and the dissolved inorganic nitrogen in the forms of ammonium, nitrite and nitrate. The ecosystem model is able to simulate successfully main observed features and trends of the intense eutrophication phase (from the early 1970s to the early 1990s), but points to its modification to simulate better the ecosystem conditions of the post-eutrophication phase.

1 Introduction

The Black Sea is one of the largest enclosed basins in the world, which has been receiving relatively high nutrient load from rivers draining parts of Europe and Asia. The Black Sea marine ecosystem manifested significant changes since the 1960s in response to the nutrient enrichment, overfishing and large population growth of gelatinous and opportunistic species. These changes altered severely biomass, taxonomic composition, and community structure of plankton groups particularly in the northwestern shelf. The classical phytoplankton annual cycle with spring and autumn maxima in biomass has been modified by additional blooms – the summer one being the most pronounced. These changes in the food web structure were also accompanied by modifications in the vertical geochemical structure. The most evident ones were an increase of nitrate concentration in the nitracline zone from 2 to 3 $\mathrm{mmol\,m^{-3}}$ in the late 1960s to 6–9 $\mathrm{mmol\,m^{-3}}$ during the 1980s and broadening of the suboxic zone (Konovalov and Murray, 2001).

The ecosystem dynamics and its reorganisations during different phases of the ecosstem changes of the Black Sea have been studied by a series of one-dimensional coupled physical-biogeochemical models (Oguz et al., 2000, 2001, 2008; Lancelot et al., 2002; Gregoire et al., 2008). Their three-dimensional extensions are provided by Grégoire and Lacroix (2003), Grégoire and Friedrich (2004), Grégoire et al. (2004), Dorofeyev (2009), Korotaev et al. (2011). The present study extends these studies by employing a three-dimensional coupled physical-ecosystem model to study evolution of the ecosystem from 1971 to 2001. One particular feature of the model is the assimilation available hydrographic and current measurements into the circulation model. The period 1971–1994 involved relatively dense hydrographic surveys and was replaced by the availability of altimetry data from the Topex/Poseidon and ERS missions afterwards. Reanalysis of the Black Sea dynamics for 1971–1993 performed by Moiseenko et al. (2009) indicates that the seasonal and interannual variability of temperature, salinity and current fields are well resolved. Additional simulations with the space altimetry assimilation for 1994–2001 pointed to detailed mesoscale variability of the Black Sea circulation (Korotaev et al., 2003; Dorofeyev and Korotaev, 2004). The present paper is organized as follows. Section 2 describes main features of the model and the methodology used for the simulation experiments. Section 3 provides information about variability of temperature salinity and current fields during the three decades of the model simulations. Section 4 presents long-term evolution of the Black Sea ecosystem. The main findings are discussed in Sect. 5.

2 Methodology of simulations

2.1 Reanalysis of marine dynamics of 1971–1993

Reanalysis of the Black Sea dynamics for 1971–1993 was performed by assimilating the available temperature and salinity profiles into the circulation model (Moiseenko et al., 2009) which is based on the POM (Princeton Ocean Model) model (Blumberg and Mellor, 1987). The POM regional model includes the Mellor and Yamada level 2.5 turbulence module (Mellor and Yamada, 1982). The river discharges to the sea are taken into account in the model, as well as the water exchange with the Azov Sea through the Kerch strait and with the Marmara Sea through the Bosporus, where water flows from the Black Sea in the upper layer (upper Bosporus current) and into the Black Sea in the lower layer (lower Bosporus current). Considering the lack of knowledge on the interannual variability of the lower Bosporus flow, it is estimated by assuming that the Black Sea water volume does not changed from one year to another, i.e. annual rivers inflows, water discharges through the Bosporus and the Kerch strait and also precipitations and evaporation altogether are equal to zero.

The simulations were carried out on a horizontal rectangular grid of 8.1 km along the zonal and 6.95 km along the meridian directions. 26 σ-surfaces were used along the vertical: 0, −0.003, −0.006, −0.009, −0.012, −0.015, −0.020, −0.025, −0.030, −0.035, −0.040, −0.045, −0.050, −0.055, −0.060, −0.067, −0.075, −0.090, −0.140, −0.200, −0.330, −0.500, −0.670, −0.830, −0.910, −1.000. The coefficients of horizontal turbulent exchange of momentum, heat and salt were assumed to be: $A_M = 300\,\mathrm{m}^{-2}\,\mathrm{s}^{-1}$, $A_H = 60\,\mathrm{m}^2\,\mathrm{s}^{-1}$, respectively. The coefficients of vertical turbulent viscosity K_M and diffusion K_H are expressed through the turbulence kinetic energy and the stability parameters which are the functions of the Richardson number.

The products of Mediterranean array of global reanalysis ERA-40 created by the European Center of Mid-term Weather Forecasts ECMWF (Uppala et al., 2005) with spatial resolution 1.125° × 1.125° and temporal resolution 6 h for the period 1958–2002 was used for the atmospheric forcing of the model. They include wind direction and speed at 10 m height, temperature on the sea surface, fluxes of short-wave and long-wave radiation, and sensible and latent heats, precipitations (continuous and convective ones) and evaporation. The wind stress vector is defined using the bulk formula.

Approximately three to ten monthly hydrographic surveys per year have been conducted during 1971–1993 with irregular coverage both in space and time. The special procedure of interpolation was applied to make observations more suitable for the reanalysis. It is based on the optimal interpolation approach and climatic fields used as a base of the optimal interpolation (Knysh et al., 2008). The climatic fields on the model grid were prepared in the following way. The monthly climatic arrays of temperature and salinity (Moiseenko and Belokopytov, 2008) were first interpolated on the model grid and then temporally for each day of a year by means of harmonic functions of time. They were then assimilated in the model. The simulations were carried out on time period of 15 yr using climatic atmospheric forcing (Staneva and Stanev, 1998). The model fields demonstrated periodic oscillations at the end of integration and we have considered them as the climatic one.

Autocorrelation functions of temperature and salinity climatic fields were calculated for different directions every 10° for winter (February), spring (May), summer (August) and autumn (November) on the horizons 10, 50, 105, 200, 500, 1000 and 1500 m using the simulated climatic array (Moiseenko and Belokopytov, 2008). The spatial correlation of temperature and salinity fields is well approximated by an ellipse on all horizons and for all seasons. On all horizons and in all seasons (except for the horizon 50 m in winter), the orientation of temperature field isocorrelates is close to zonal. The large ellipse semi-axis has zonal direction and is equal ~ 330 km, the small semi-axis is equal ~ 160 km. Two-dimensional correlation functions of salinity field are stretched in zonal direction and large ellipse semi-axis is equal ~ 260 km, the small semi-axis is equal ~ 75 km. Two-dimensional correlation functions were approximated by analytical expressions.

The data selected from a strobe pulse ±45 days are used to build the monthly arrays of temperature and salinity by means of optimal interpolation. The temporal correlation function which had the exponential form was used to interpolate observations in time. Such interpolation permits us to fill the gaps when measurements were not available. Monthly fields of temperature and salinity were reconstructed on 36 horizons. Climatic temperature and salinity data are used deeper 300 m. It is important to note that the optimal interpolation method permits to evaluate a standard deviation of every interpolated value of temperature and salinity.

Monthly arrays of temperature and salinity as well as monthly fields of dispersion errors are interpolated from z-levels to the model σ-surfaces and for each time step. Then they are used for correction of temperature and salinity fields simulated by POM using the Kalman filter algorithm formalism (Gandin and Kagan, 1976). Such approach when the error statistics is evaluated a priori is usually named as the data assimilation by optimal interpolation Let us mention that the weight of the POM simulation correction depends on the standard deviation of optimally interpolated temperature and salinity fields

2.2 Reanalysis of the Black Sea dynamics in 1994–2001

Only limited number of hydrographic cruises is available between 1994 and 2002. Nevertheless, the Topex/Poseidon and ERS space altimetry missions started from 1992. We therefore employed the merged sea level anomaly (SLA) products provided by AVISO service to reconstruct the basin-scale dynamics between 1994 and 2002. SLA is converted to the sea surface height (SSH) by adding the climatic sea surface topography obtained from the assimilation of the climatic temperature and salinity arrays in POM as described by Korotaev et al. (2001). Along-track SSH profiles are assimilated into the POM using optimal interpolation method. The correlation of SSH with temperature and salinity variations is evaluated using the eddy-resolving runs of the POM.

2.3 The Black Sea ecosystem model

The ecosystem model consists of the physical and biogeochemical parts. The physical part involves the circulation based on POM (Princeton Ocean Model), driven by ERA40 atmosphere forcing. It has 26 sigma levels compressed towards the surface. Boundary conditions on the sea surface are heat and fresh water fluxes and surface temperature, provided by data set from atmosphere model every 6 h.

The biogeochemical model is an extension of the ne-dimensional model given by Oguz et al. (2000, 2001, 2008) using identical parameters. It has one-way off-line coupling with the circulation model through current velocity, temperature, salinity and turbulent diffusivity. The biogeochemical model extends to 200 m depth with 26 z-levels, compressed to the sea surface. It includes 15 state variables. Phytoplankton is represented by two groups, typifying diatoms and flagellates. Zooplankton is also divided into two groups: microzooplankton (nominally < 0.2 mm) and mesozooplankton (0.2–2 mm). The carnivorous zooplankton group covers the jellyfish *Aurelia aurita* and the ctenophore *Mnemiopsis leidyi*. The model food web structure also includes the omnivorous dinoflagellate *Noctiluca scintillans* as an additional species group. It is a critical species at an intermediate trophic level and feeds on phytoplankton, bacteria, microzooplankton, and particulated organic matter, and is consumed partly by mesozooplankton, but generally acts as a dead-end of the food web. The model further includes nonphotosynthetic free living bacteriaplankton, detritus and dissolved organic and inorganic nitrogen. The latter has the forms of forms of nitrate, nitrite and ammonium. Nitrogen is considered as the only limiting nutrients for phytoplankton growth and state variables are expressed in the unit of mmol N m^{-3}. Additional components of the biogeochemical model are dissolved oxygen and hydrogen sulfide. The local temporal variations of all variables are expressed by equations of the general form

$$\frac{\partial F}{\partial t}+\frac{\partial (uF)}{\partial x}+\frac{\partial (vF)}{\partial y}+\frac{\partial ((w+w_s)F)}{\partial z}=K_h\nabla^2 F+\frac{\partial}{\partial z}\left(K_v\frac{\partial F}{\partial z}\right)+\Re(F),$$

where $\Re(F)$ includes the biological interaction terms among the state variables F; w_s represents the sinking velocity for diatoms and detrital material and is set to zero for other compartments; (u, v, w) – components of the current velocity, K_h, K_v – horizontal and vertical coefficients of turbulent diffusion provided by the physical model. The horizontal grid resolution is approximately 7 km.

The circulation model provides the input to the biological model from the assimilation of the archive hydrography data for the first twenty three years, and then of assimilation of the space altimetry (AVISO product) for the latter 8 yr. Fluxes of all biogeochemical variables are set to zero at the sea surface, and the bottom in shallow part of the basin and along the lateral boundaries, except rivers estuaries where the nitrate fluxes are set up as the product of rivers discharges and nitrate concentrations (Ludwig, 2007). On the lower liquid boundary in the deep part of the basin the concentrations of all state variables set to zero except ammonium and hydrogen sulfide (sulfide and ammonium pools).

3 Interannual and seasonal variability of circulation dynamics

The reanalysis data collected every five days are used for the analysis of interannual and seasonal variability of temperature, salinity and kinetic energy (KE). To consider their temporal evolutions the data were averaged over the whole basin at different depth levels. Interannual variability is evaluated on the basis of annual-mean temperature, salinity and KE.

3.1 Interannual and seasonal variability of temperature field

Simulation shows rather significant interannual variability of temperature field. Even averaged over the basin volume temperature demonstrates changes of annual minimums and maximums in the range of 0.05 °C (Fig. 1). Figure 1 shows that the basin-average temperature was minimal in winter of 1993 whereas the highest basin-averaged winter temperature was in 1981. Lowest summer maximum was observed in 1976 year and highest in 1981 and 1984 years.

Such characteristics of the thermohaline structure as the autumn-winter cooling and spring-summer heating of surface waters, formation of the upper mixed layer (UML) and the seasonal thermocline, renewal of the cold intermediate layer (CIL) and formation of a new CIL, decrease of cold reserve in CIL by autumn are resolved by model simulations.

The UML depths vary within 20–64 m (based on isotherms 7 °C). The increased thickness of the upper mixed layer (up to ~ 54 m) was observed in 1976, 1985, 1987, 1989 and 1992. The maximal depth of the mixed layer (~ 64 m) was marked in 1993 which is known to be one of the coldest years of the 20th century.

The CIL upper and lower boundaries are identified based on location of isotherm 8 °C. The CIL thickness diminishes during spring-summer mainly due to deepening of its upper boundary resulting from the surface water heating, vertical advection and turbulent heat diffusion. The changes in vertical temperature structure below the CIL follows the seasonal and interannual variability of CIL lower boundary.

Following the classification suggested by (Titov, 2003), 1987 and 1989 are characterized by normal conditions whereas 1976, 1985, 1992 and 1993 corresponds to the cold winters. As shown in Fig. 2, during the cold winter of 1993 extreme cooling was on the sea surface and the CIL cold reserve as well as its thickness turned out to be greater than in other years. Anomalously high heat fluxes on the air-sea boundary in winter also influence CIL behavior. In particular average temperature on all levels in the layer 0–300 m in autumn exceeds 8 °C in 1971, 1972, 1975, 1977, 1980–1982 and 1984 which is the result of considerable total heat inflow. The CIL continuity was violated on some levels in these years (Fig. 3). On the whole the CIL thickness tended to increase in 1985–1994.

Summer 1981 (enormously warm winter conditions according to Titov, 2003) temperature on the level 50 m was substantially higher and the CIL thickness and cold reserve were smaller than in summer 1987 (normal winter conditions). Average temperature in warm 1981 on the level 50 m exceeded climatic values during almost the whole year (except for October–December). In cold 1993 year the temperature in the course of a seasonal cycle was much lower than the climatic one.

Analysis of tendencies of interannual variability of the temperature average over a year reveals the following (Fig. 4). In the layers 0–50 and 50–100 m linear trends of variability are negative that agrees with the tendency of variability of annual average total heat flux. An average temperature decrease in those layers is equal -2.57×10^{-2} and $-1.03 \times 10^{-2}\,°\mathrm{C\,yr^{-1}}$, respectively. Rather weak, but positive trend is observed in the layer 100–300 m. An average temperature is characterized by a pronounced positive trend in deeper layers (500–1000 m).

Temperature in the Black Sea is influenced by many factors: heat fluxes through the surface and lateral sea boundaries; horizontal and vertical mixing; convection and wind mixing in autumn-winter period; summer upwelling and others. To study long-term variability of the vertical stratification we calculated differences between annual temperature and salinity values averaged on horizons 100 and 50 m, and also on levels 200 and 50 m in the maximally stratified part of pycnocline. On the whole the noted temperature differences increased in 1971–1993, and salinity differences – in 1971–1985. Evident temperature increase on horizon 200 m and deeper can be explained by strengthening of stratification and decrease of the heat flux through the layer of high density gradients. The same results were obtained in (Belokopytov and Shokurova, 2005) at studying of decadal variability of difference between the averaged values of temperature and salinity on the same levels in 1970–1990.

3.2 Interannual and seasonal variability of salinity

An averaged over the basin volume salinity also shows visible changes mainly on interannual scale (Fig. 5). Seasonal cycle does not manifested clearly probably because the deep salinity is controlled by the lower Bosphorus current.

Analysis of the salinity distribution in the layer 0–300 m shows that a seasonal signal is traced in the whole layer (Fig. 6). Smallest salinity values (less 18 ‰) are observed in the upper layer with thickness ~ 10–20 m. In 1976 (cold winter conditions) average over the sea surface value of salinity was maximal and equal 18.4 ‰. The salinity of surface water diminishes noticeably starting from 1977. Based on climatic data and those on separate years, maximal salinity in its seasonal variation falls on February. Minimal salinity is observed in the late June and is a result of spring river floods; from July salinity of surface waters begins to grow.

Analysis of tendencies of interannual variability of the layer-average salinity permitted to reveal the following regularities (Fig. 7). Negative linear salinity trend is observed in the upper part of halocline (0–20 m). The characteristic of the trend is equal to -0.89×10^{-2} ‰ yr^{-1}. Tendency of the layer-average salinity in permanent halocline (20–150 m) is opposite to that observed in the layer 0–20 m. The increase of average salinity in the layer 20–150 m achieves 0.16×10^{-2} ‰ yr^{-1}. The local salinity minimum is distinguished in 1982 on a general positive tendency.

Interannual salinity variability in the layers 150–300 and 500–1000 m is characterized by positive linear trends with inclinations 0.24×10^{-2} and 0.2×10^{-4} ‰ yr^{-1}, respectively. A general positive tendency of salinity variation in the layer 150–300 m is accompanied by three local maximums in 1973, 1980 and 1988 years. Major contribution to the inter-annual variability of volume-average salinity is brought by the interannual salinity variability in a permanent halocline.

Temporal variability of annual mean salinity in the upper layer is defined by many factors: water exchange through the Bosporus and the Kerch strait; rivers' inflows; precipitations; evaporation; intensity of seawater mixing in winter period by the convective and wind mixing. Freshwater balance had a positive linear trend in 1951–1985 (Hydrometeorology and hydrochemistry, 1991). According to Lipchenko et al. (2006) in 1951–1995 evaporation decreased. The atmospheric precipitations (in annual values) on the Black Sea surface grew in 1923–2005 (Repetin et al., 2006). At the same time the trend of rivers' inflow appeared to be not significant. It is possible to conclude on the base of presented estimations that the fresh water balance also had a positive trend in 1951–1995. Exactly this factor explains negative tendency of temporal variability of annual salinity values in the upper layer 0–50 m.

Interannual variability of salinity in the Black Sea in a permanent halocline mainly depends on temporal variability of discharges and salinity of the Marmara Sea waters flowing to the sea through the Bosporus strait. By present there is no reliable information about interannual variability of the mentioned above factors. Salinity increase below 50 m can be related to the positive salinity trend in the Mediterranean Sea (Thimplis et al., 2004). Intensification of the deep water upwelling on the lower boundary of permanent halocline resulted in its rise is also possible reason of salinity increase in the upper layers and observed sharpening of pycnocline in 1971–1985.

3.3 Interannual and seasonal variability of the basin-scale circulation

Seasonal variability of kinetic energy during a year is definitely traced (Fig. 8). It is substantially lower in summer than in winter. The highest intensity of water circulation in the layer 0–300 m is observed in February–March, the lowest – in September–October. It is known that wind is a leading factor in formation of the Black Sea currents (Korotaev, et al., 2001). Peculiarities of seasonal variability of the average over the sea surface wind stress vorticity are conditioned the seasonal variability of the averaged KE.

Interannual variability of annual mean, layers-averaged KE is characterized by the positive linear trends in the layers 0–50 and 50–150 m. The trends have the following characteristics: 3.41×10^{-6} and $3.49 \times 10^{-6}\,\mathrm{M}^2\,\mathrm{c}^{-2}\,\mathrm{yr}^{-1}$, respectively. The KE is diminished by $1.25 \times 10^{-6}\,\mathrm{M}^2\,\mathrm{c}^{-2}\,\mathrm{yr}^{-1}$ in the layer 200–300 m.

Changes of kinetic energy on the levels 50, 75, 100 and 150 m show the years with its lower (1974, 1978, 1980, 1983, 1986 and 1990) and higher (1972, 1977, 1981, 1988, 1991 and 1993) annual values. Intensity of winter water circulation in these years decreased or increased, respectively. The maps of currents for the years of stronger circulation intensity demonstrate more intense Rim current and more pronounced Kizilirmak Batumi, Caucasian, Sevastopol, Kaliakra and Bosporus anticyclonic vortices.

4 Evolution of the Black Sea ecosystem

Evolution of the annual-mean phytoplankton biomass in the upper 50 m layer derived from the modeling for the deep part of the Black Sea basin and North Western Shelf is shown in Fig. 9. In the deep part of the basin phytoplankton biomass increased approximately twice from about 1.2 $\mathrm{g\,C\,m^{-2}}$ in early seventies to 2 $\mathrm{g\,C\,m^{-2}}$ during the early 1980s that prevailed throughoutt the 1980s and the early 1990s and then experienced a declining trend. On the northwestern shelf the level of the phytoplankton biomass in general is about one and half times as large as in the deep part of the basin. It also increased from about 2 $\mathrm{g\,C\,m^{-2}}$ during the early seventies to 3 $\mathrm{g\,C\,m^{-2}}$ in the mid-eighties. Then it decreased back to 2 $\mathrm{g\,C\,m^{-2}}$ until 1994 followed by an abrupt rising during the rest of the 1990s. In general the phytoplankton biomass was higher in the western interior basin during the 1970s and the early1980s due to lateral support from the northwestern shelf. This excess biomass however became negligible during the reduced phytoplankton production phase of the northwestern shelf during 1985–1995.

Interannual variability of the zooplankton biomass in the upper 50 m layer as a result of the modeling is represented separately for the deep part of the Black Sea basin and North Western Shelf region in Fig. 10. In response to the phytoplankton biomass increase in deep part of the basin, zooplankton biomass increased from about 0.8 $\mathrm{g\,C\,m^{-2}}$ in early seventies to about 1.1 $\mathrm{g\,C\,m^{-2}}$ in 1987. Then zooplankton biomass reduced rapidly in 1998 and stabilizes on the level of about 0.7 $\mathrm{g\,C\,m^{-2}}$. Zooplankton biomass on the northwestern shelf was retained uniform about 1.2 $\mathrm{g\,C\,m^{-2}}$ until 1987, and reduced abruptly as well to about 0.7 $\mathrm{g\,C\,m^{-2}}$. This sudden decrease in zooplankton population in late eighties was caused by the population outbreak of *Mnemiopsis leidyi* all over the Black Sea. The *Mnemiopsis leidyi* invasion during 1989–1991 altered the previous carnivore predation of *Aurelia aurita* (Fig. 11).

The surface layer in the deep part of the Black Sea was supplied by nutrients from immediately below the euphotic zone (60–80 m depths) in which nitrate concentration increased from 2–3 $\mathrm{mmol\,N\,m^{-3}}$ in the 1960s to 8–9 $\mathrm{mmol\,N\,m^{-3}}$ in the late 1980s.

Nitrate concentration in this layer then decreased to about 4 mmol N m^{-3} in late 1990s–early 2000s due to the reduction in the anthropogenic nutrient supply (Konovalov and Murray, 2001). Apart from an increase in the value of the nitrate maximum by about three times during 20 yr (from the early 1970s until the end of 1980s) the position of nitrate peak shifted by about 10 m upward. During winter season the nitrate accumulated in the upper layer due to intense winter mixing and then assimilated by phytoplankton once the spring warming initiated.

Figure 12 demonstrates variability of the basin-averaged surface phytoplankton and nitrate concentrations computed by the model in the deep part of the Black Sea together with its concentration in the layer of nitrate maximum (dots). The annual-mean surface nitrate concentration increased five times from 0.4 mmol N m^{-3} in the early seventies to about 2.5 mmol N m^{-3} in the early nineties, and then it decreased later by half. The surface phytoplankton concentration also increased from from 0.2 mmol N m^{-3} during the early 1970s to from 0.7 mmol N m^{-3} in 1991. Then it reduced to 0.3 mmol N m^{-3}. Both the surface nitrate concentration and the surface phytoplankton biomass followed closely the changes in the concentration of nitrate maximum layer.

On the northwestern shelf of the Black Sea, nutrient concentrations were influenced mainly by the supply from the rivers (mainly Danube which provided about 70 % of total nutrient) (see Fig. 13, left). The surface phytoplankton biomass changed around 1.1 mmol N m^{-3} during the first twenty years, and declined abruptly during 1992–1994 and increased afterwards. But no clear correlation is evident with the anthropogenic nutrient supply as in the case of surface nitrate. It seems to be due to the fact that phytoplankton production was limited by other factors that the nitrate concentration in the northwestern shelf.

In more details, well-pronounced winter peaks of the basin-averaged surface nitrate and phytoplankton for the deep part of the Black Sea are presented on Fig. 14. Due to strong winter mixing nitrate concentration accumulates into the surface layer from the nitracline, and are consumed by phytoplankton subsequently at the end of winter and early spring at the end of the winter mixing season. The surface nitrate concentration becomes at negligible quantities until the next winter. Apart from the seasonal changes, interannual variability of the nitrate and phytoplankton peaks is also well pronounced in Fig. 14. Their values are more clearly depicted in Fig. 15. From the early-1970s to the early 1990s, the winter nitrate maximum increases by about four times from 2 mmol N m^{-3} to 8 mmol N m^{-3}. Then it decreases to the value of about 3 mmol N m^{-3}. The mean spring phytoplankton biomass closely follows the winter nitrate concentration, and rises from 0.35 mmol N m^{-3} in 1971 to 0.9 mmol N m^{-3} in 1991. Afterwards they tend to switch to the declining trend.

The changes in the Black Sea ecosystem during time period from 1971 until 2001 are visible not only in interannual changes of the main ecosystem components, but also in their seasonal variability. The natural phytoplankton annual cycle of the spring and autumn blooms, as typical for the pre-eutrophication phase of the Black Sea ecosystem, has been replaced by a more complicated seasonal structure identified by several maxima, as illustrated by, the phytoplankton, zooplankton and medusa *Aurelia aurita* changes in the upper 100 m layer in the central part of the basin for 1972, 1982 and 1992 in Fig. 16. In 1972, the phytoplankton annual cycle involved only the spring and autumn maxima in biomass. The zooplankton peak followed closely that of phytoplankton with some time lag of about half a month. The jellyfish *Aurelia aurita* acquired two pronounced maxima in April–May and late autumn. In 1982 (the intense eutrophication phase), the phytoplankton annual cycle included additional peaks. Phytoplankton experienced a major bloom during the late winter-early spring season that was first followed by a zooplankton bloom of comparable intensity, which reduced the phytoplankton stock to a relatively low level, and then by an *Aurelia* bloom in the late spring early summer that similarly reduced the zooplankton biomass. Subsequently, phytoplankton biomass recovered and produceed a relatively weak late spring bloom. The *Aurelia* population produced a second peak in September–November and were accompanied by relatively high biomass of phytoplankton and zooplankton.

The period after 1988 (*Mnemiopsis* invasion into the Black Sea) constituted the new phase in the Black Sea ecosystem dominated by strong grazing pressure by

Mnemiopsis community. The sudden increase in *Mnemiopsis* population led to a reduction in zooplankton biomass as well as an abrupt decline in the *Aurelia* biomass. Phytoplankton produced a set of maxima with the summer one is being the most-pronounced. The largest growth of the zooplankton was observed during mid-spring.

Apart from the bottom-up and top-down controls, intensity of the primary production in the euphotic zone depends also on climatic conditions. The upper layer in deep part of the Black Sea is supplied with nutrients mainly by the winter mixing, the intensity of which depends on the severity and frequency of winter storms and cooling. The lower winter temperature is therefore associated with deeper winter convection and, as a result, more nutrient entrainment from its subsurface pool. Figure 17a displays the basin-averaged annual-mean and winter-mean sea surface temperature changes obtained from the results of the hydrodynamic model. During the first phase (1971–1993), both the annual and winter-mean temperature tended to have a declining trend (i.e. cooling) until their minimum in 1992 and 1993. Then they switched to the warming trend with the SST rise of about 2 °C from 1993 to 2001. In addition an opposite correlation between winter surface nitrate concentration and winter-mean SST is evident in Fig. 17b. More details on the process of upper layer enrichment in winter season can be illustrated by the long-term changes in water column nitrate concentration during 1988–1994 at a location chosen from the interior Black Sea (Fig. 18). The most pronounced feature is an increase in the surface layer nitrate concentration due to higher rate of input from nitracline due to intense winter mixing. The coldest winters in 1992 and 1993 provided the highest intensity winter surface nitrate concentration.

Satellite color scanners provide a good opportunity to validate the modeling results. For example, Fig. 19 compares the basin averaged surface chlorophyll concentration for the deep part of the basin derived from the modeling (solid line) and the SeaWiFS data (dotted line) for 1998–2001 (http://blackseacolor.com). Their main difference emerges for the shift in the winter–spring peak. The model provided this peak in the early spring, but the satellite data show its presence during the mid winter. This issue demands more study to elaborate whether it is related to the climatic changes (warming tendency) or the changes in trophic interactions during the post-eutrophication phase of the ecosystem. Nevertheless, the model predicts a annual-mean surface chlorophyll concentration reasonably well and close to that given by the SeaWiFS data. Comparison of seasonal composite images of the surface chlorophyll provided by the SeaWiFS data and results of the modeling is shown in Fig. 20. The averaging was done over four year time period 1998–2001. As indicated above, the model underestimated the autumn and winter concentrations and vice versa for the spring period. In summer, the difference is most observed in eastern part of the Black Sea.

The annual-averaged maps of surface chlorophyll for four years (1998–2001) presented in Fig. 21 reveal highest chlorophyll concentration within the northwestern shelf. Relatively high concentrations are also observed along the periphery of the basin due to the advection from the source in the northwestern shelf by the coastal current system of the basin scale cyclonic circulation. The mean level of surface chlorophyll derived from model agrees well with the SeaWiFS data, except the northwestern shelf where the model produces a wider coverage of high chlorophyll concentration coastal zone. It may be due to the crude resolution of very complex trophic interactions by the model.

5 Discussion

The 3-D ecological model simulations presented here displayed the main features of the long-term (1971–2001) pelagic Black Sea ecosystem characteristics fairly well. The phytoplankton biomass was shown to increase from the early 1970s to the early 1990s that represented the eutrophication phase of the Black Sea ecosystem. The surface phytoplankton biomass in the deep part of the basin increased by about 3 times. Zooplankton concentration also increased until the end of 1980s when the *Mnemiopsis* invasion caused a sudden reduction in the zooplankton community. These changes in the food web structure followed the changes in vertical chemical structure characterized by a strong increase of nitrate concentration in the layer of its maximum at approximately 70 m depth. Comparison of the model results with satellite ocean color scanner measurements was quite satisfactory except a shift of the spring bloom to the winter during the late 1990s. Reasonably good consistency between the model simulations and the general knowledge of the Black Sea ecosystem changes inferred from the available data during last three decades of the 20th century suggests the critical importance of winter vertical mixing and advection processes that govern the amount of nutrient supply into the euphotic zone and the subsequent intensity of plankton production. This climate-related process was further supported by the changes in the sea surface temperature. The intensity of upward nutrient flux is also related to the long-term accumulation of nitrate into the nitracline layer during the intense eutrophication phase. Majority of interannual changes in phytoplankton biomas may be explained by nitrate concentration in the nitracline. Our simulations do not however provide a direct link between the nutrient supply from the River Danube and the intensity of phytoplankton blooms within the interior basin. The Danube influence on the nutrient supply was limited to the northwestern shelf The *Mnemiopsis* population outbreak was manifested mainly by the suppression of the zooplankton community and some shifts on the timing of phytoplankton blooming periods, but its contribution to the phytoplankton community appears to be weaker than that predicted by the one-dimensional counterpart of the model (see Oguz et al., 2001). The model used in the present work appears to simulate the observed characteristic features of the intense eutrophication phase reasonably well, but not equally well for the post-eutrophication phase. It is related to the transient character of the Black Sea ecosystem that keeps changing at a decadal time scale under different environmental perturbations and external stressors. It points to the necessity of some modifications in the physiological characteristics of the model as well as the food web interactions and feedback processes to coup with these external changes such as climatic warming, and changes in bottom-up control and trophic cascade processes.

References

Belokopytov, V. N. and Shokurova, I. G.: Estimation of temperature and salinity interdecadal variability in the Black Sea during time period 1951–1995, Ecological safety of coastal and shelf zone and complex use of their resources, 12, 12–21, 2005 (in Russian).

Blumberg, A. F. and Mellor, G. L.: A description of a three-dimensional coastal ocean model, three dimensional shelf models, Coast. Estuar. Sci., 5. 1–16, 1987.

Dorofeyev, V. L.: Modeling of the decadal evolution of the Black Sea ecosystem, Mar. Hydrophys. J., 6, 71–81, 2009 (in Russian).

Dorofeyev, V. L. and Korotaev, G. K.: Satellite altimetry assimilation in eddy-resolved model of the Black Sea circulation, Ukr. J. Mar. Res., 1, 52–68, 2004.

Simonov, A. I. and Altman E. N.: Hydrometeorology and hydrochemistry of the seas surrounded USSR, Gidrometeoizdat, St. Petersburg, 240 pp., 1991.

Gandin, L. S. and Kagan, R. A.: Statistical methods for interpretation of the meteorological data, Gidrometeoizdat, Leningrad, 357 pp., 1976 (in Russion).

Gregoire, M. and Friedrich, J.: Nitrogen budget of the North-Western Black Sea shelf as inferred from modeling studies and in-situ benthic measurements, Mar. Ecol. Progr. Ser. 270, 15–39, 2004.

Gregoire, M. and Lacroix, G.: Exchange processes and nitrogen cycling on the shelf and continental slope of the Black Sea basin, Global Biogeochem. Cy., 17, 4201–4217, 2003.

Gregoire, M., Nezlin, N., Kostianoy, A., and Soetaert, K.: Modeling the nitrogen cycling and plankton productivity in an enclosed environment (the Black Sea) using a three-dimensional coupled hydrodynamical – ecosystem model, J. Geophys. Res., 109, C05007, 2004.

Gregoire, M., Raick, C., and Soetaert, K.: Numerical modeling of the Central Black Sea ecosystem functioning during the eutrophication phase, Progr. Oceanogr., 76, 286–333, 2008.

Konovalov, S. K. and Murray J. W.: Variations in the chemistry of the Black Sea on a time scale of decades (1960–1995), J. Mar. Syst., 31, 217–243, 2001.

Knysh, V. V., Kubryakov, A. I., Moiseenko, V. A., Belokopytov, V. N., Inyushina, N. V., and Korotaev, G. K.: Trends in thermohaline and dynamical characteristics of the Black Sea as a result of reanalysis for time period 1985–1994, Ecological safety of coastal and shelf zone and complex use of their resources, 16, 279–290, 2008 (in Russian).

Korotaev, G. K., Saenko, O. A., and Koblinsky, C. J.: Satellite altimetry observations of the Black Sea level, J. Geophys. Res., 106, 917–933, 2001.

Korotaev, G. K., Oguz, T., Nikiforov, A. A., and Koblinsky, C. J.: Seasonal, interannual and mesoscale variability of the Black Sea upper layer circulation derived from altimeter data, J. Geophys. Res., 108, 3122, doi:10.1029/2002JC001508, 2003.

Wright, D. G., Pawlowicz, R., McDougall, T. J., Feistel, R., and Marion, G. M.: Absolute Salinity, "Density Salinity" and the Reference-Composition Salinity Scale: present and future use in the seawater standard TEOS-10, Ocean Sci., 7, 1–26, doi:10.5194/os-7-1-2011, 2011.

Mellor, G. L. and Yamada, T.: Development of a turbulence closure model for geophysical fluid problem, Rev. Geophys. Spase Phys., 20, 851–875, 1982.

Lancelot, C., Staneva, J., Van Eeckhout, D., Beckers, J., and Stanev, E.: Modelling the danube-influenced north-western continental shelf of the Black Sea. II: ecosystem response to changes in nutrient delivery by danube river after its damming in 1972. Estuar. Coast. Shelf Sci., 54, 473–499, 2002.

Lipchenko, A. E., Ilyin, Y. P., Repetin, L. I., and Lipchenko M. M.: Decrease of evaporation from the Black Sea surface in the second half of the 20th century as a result of the global climate changes, Ecological safety of coastal and shelf zone and complex use of their resources, 14, 449–461, 2006 (in Russian).

Ludwig W.: River runoff and nutrient load data synthesis for hindcasting simulations, Deliverable 4.3.2, SESAME project, 2007.

Moiseenko, V. A. and Belokopytov, V. N.: Quality control of the hydrological data prepared for reanalysis of the Black Sea state during the time period of 1971–1993, Ecological safety of the coastal zone and complex use of the shelf resources, 16, 184–189, 2008.

Moiseenko, V. A., Korotaev, G. K., Knysh, V. V., Kubryakov, A. I., Belokopytov V. N., and Inyushina, N. V.: Interannual variability of the thermohaline and dynamical characteristics of the Black Sea according to reasults of the reanalysis for time period 1971–1993, Ecological safety of the coastal zone and complex use of the shelf resources, 19, 216–227, 2009 (in Russian).

Oguz, T., Ducklow, H. W., and Malanotte-Rizzoli P.: Modeling distinct vertical biochemical structure of the Black Sea: dynamical coupling of the oxic, suboxic, and anoxic layers, Global Biochem. Cy., 14, 4, 1331–1352, 2000.

Oguz, T., Ducklow, H. W., Purcell, J. E., and Malanotte-Rizzoli P.: Modeling the response of top-down control exerted by gelatinous carnivores on the Black Sea pelagic food web, J. Geophys. Res., 106, 4543–4564, 2001.

Oguz, T., Salihoglu, B., and Fach, B.: A coupled plankton-anchovy population dynamics model assessing nonlinear controls of anchovy and gelatinous biomass in the Black Sea, Mar. Ecol. Prog. Ser., 369, 229–256, 2008.

Purcell, J. E., Shiganova, T. A., Decker, M. B., and Houde, E. D.: The ctenophore mnemiopsis in native and exotic habitats: US estuaries versus the Black Sea basin, Hydrobiologia, 451, 145–176, 2001.

Repetin, L. I., Dolotov, V. V., and Lipchenko, M. M.: Space, temporal and climatic variability of the atmospheric precipitation over the Black Sea region, ecological safety of coastal and shelf zone and complex use of their resources, Sevastopol, 14, 462–476, 2006 (in Russian).

Staneva, J. V. and Stanev, E. V.: Oceanic response to atmospheric forcing derived from different climatic data sets, intercomparison study for the Black Sea, Oceanol. Ac., 21, 3, 383–417, 1998.

Titov, V. B.: Influence of climatic multiannual variability on the hydrological structure and interannual renewal of the cold intermediate layer in the Black Sea, Oceanology, 43, 176–184, 2003 (in Russian).

Thimplis, M. N., Josey, S. A., Rixen, M., and Stanev, E. A.: On forcing of sea level in the Black Sea, J. Geophys. Res., 109, C08015, 2004.

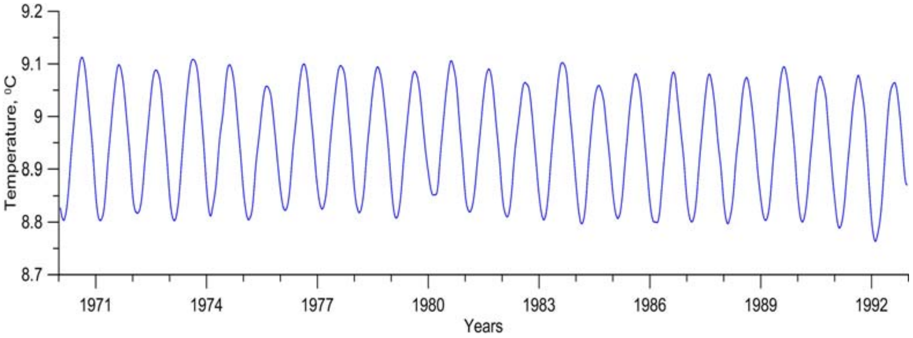

Fig. 1. Interannual and seasonal variability of the volume averaged temperature.

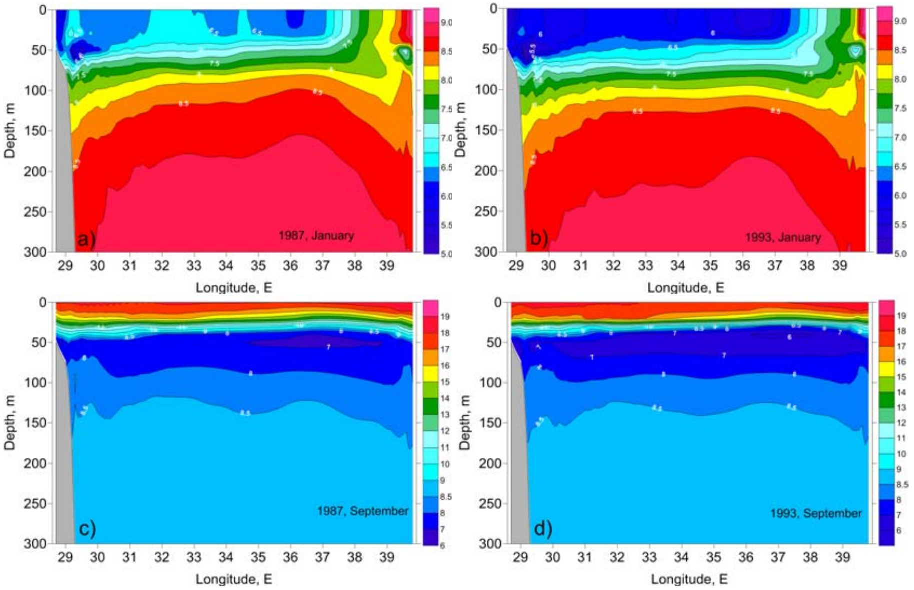

Fig. 2. Vertical sections of the temperature field along 43°30′ N in January (upper row) and September (bottom row) in normal conditions of 1987 (left) and cold conditions of 1993 (right).

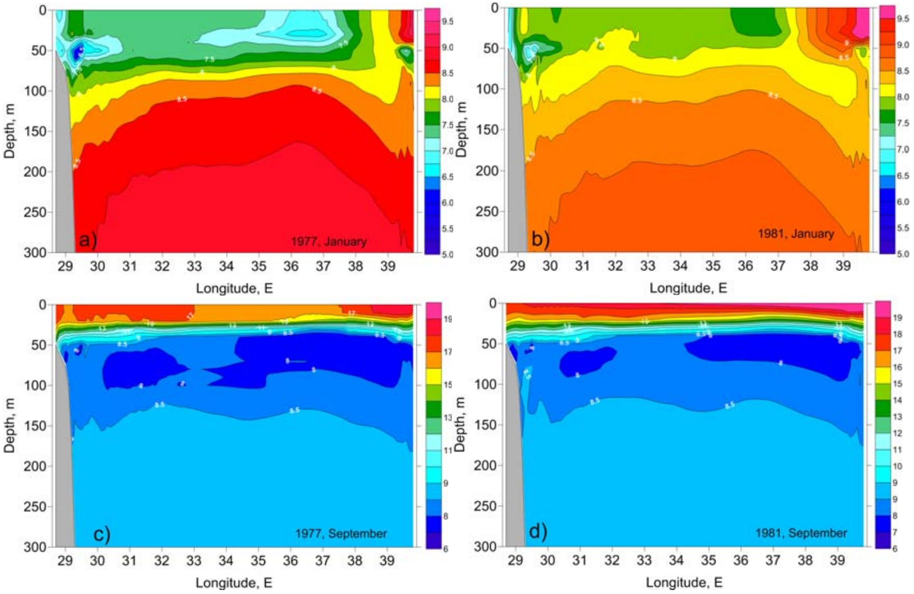

Fig. 3. Vertical sections of the temperature field along 43°30′ N in January (upper row) and September (bottom row) in warm weather conditions of 1977 (left) and very warm conditions of 1981 (right).

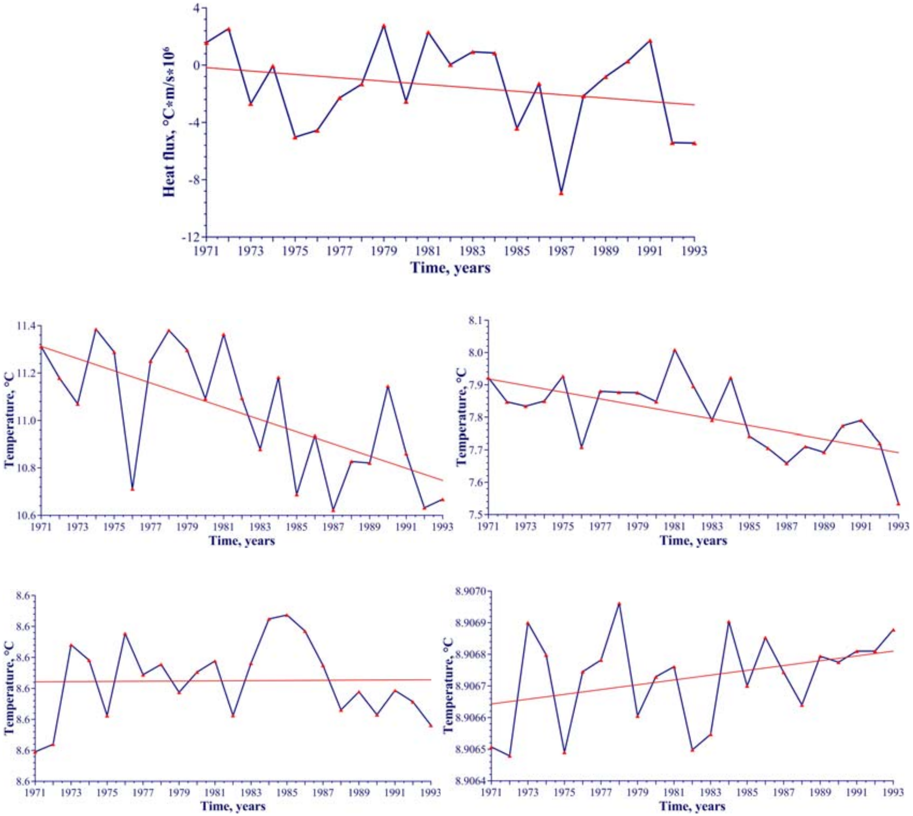

Fig. 4. Interannual variability of averaged over the sea surface of total heat flux from atmosphere **(a)** and interannual variability of temperature averaged in the layer 0–50 m **(b)**, 50–100 m **(c)**, 100–300 m **(d)**, 500–1000 m **(e)**. The strait lines show linear trends.

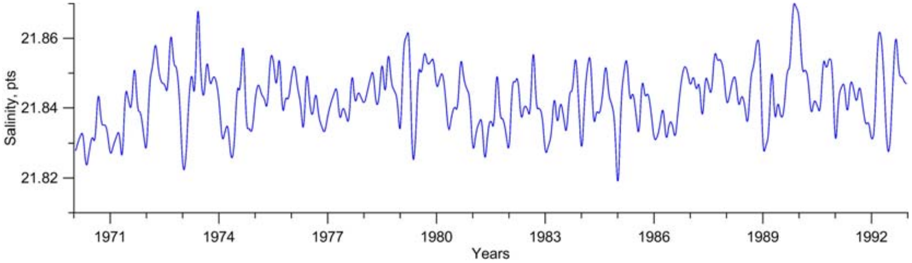

Fig. 5. Interannual and seasonal variability of a volume averaged salinity.

Title Page
Abstract | Introduction
Conclusions | References
Tables | Figures
◀| |▶
◀ ▶
Back | Close
Full Screen / Esc
Printer-friendly Version
Interactive Discussion

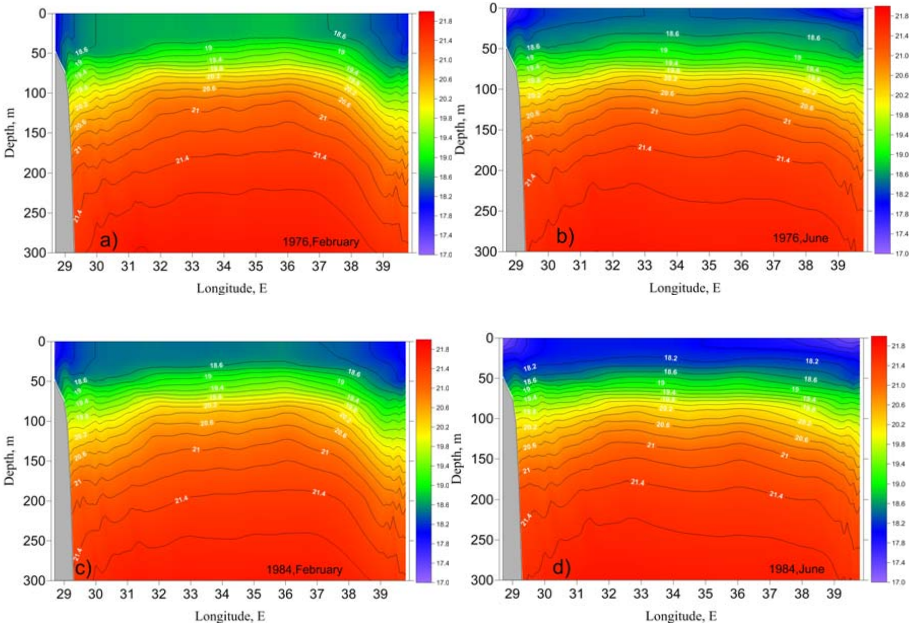

Fig. 6. Salinity sections along 43°30′ N in 1076 (upper panel) and 1984 (bottom panel) years corresponding to cold and warm winters.

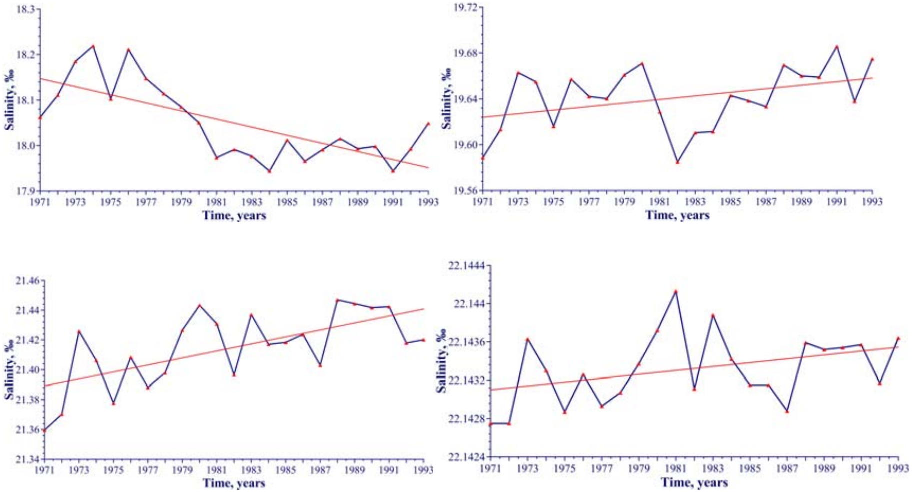

Fig. 7. Interannual variability of salinity averaged in the layer – 20 m **(a)**, 20–150 m **(b)**, 150–300 m **(c)**, 500–1000 m **(d)**.

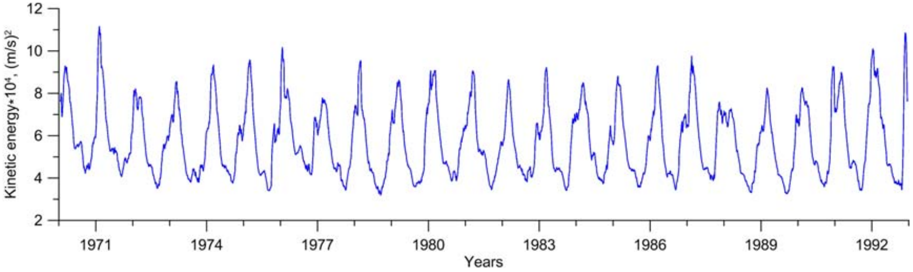

Fig. 8. Interannual and seasonal variability of a volume averaged kinetic energy.

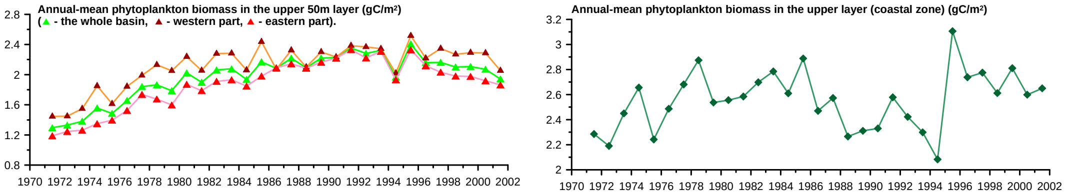

Fig. 9. Evolution of the annual-mean phytoplankton biomass in the upper 50 m layer for the deep part of the Black Sea basin (left) and North Western Shelf (right). On the left plot brown triangles denote values of the phytoplankton biomass for western part of the interior basin, red triangles – for eastern part, and green – for the whole deep part of the basin. The biomass is converted to carbon unit by assuming 1 mmol N roughly equal to 0.1 gC.

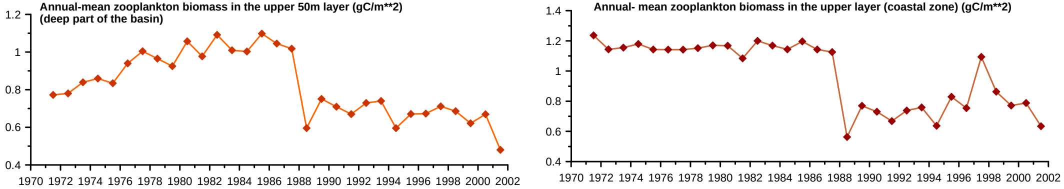

Fig. 10. Evolution of the annual-mean zooplankton biomass in the upper 50 m layer for the deep part of the Black Sea basin (left) and North Western Shelf (right).

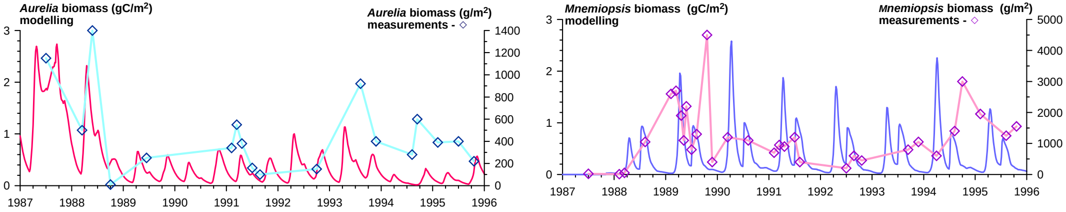

Fig. 11. Evolution of the Aurelia (left) and Mnemiopsis (right) biomass in the upper 50 m layer for the deep part of the Black Sea: results of the modeling and measurements (squares) (Purcell et al., 2001).

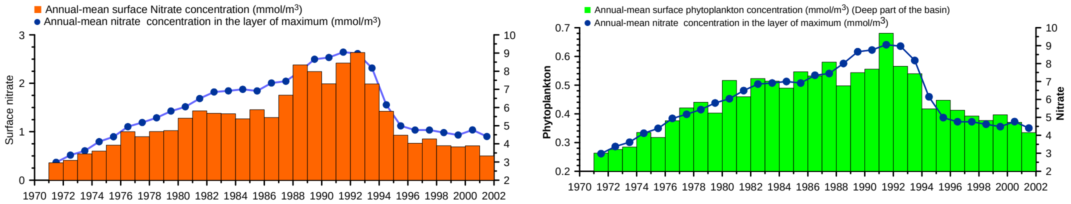

Fig. 12. Annual-mean surface nitrate (left) and phytoplankton (right) concentrations (bars) in the deep part of the Black Sea and annual-mean nitrate maximum (dots) (results of the modeling).

Title Page
Abstract
Introduction
Conclusions
References
Tables
Figures
◀❙
❙▶
◀
▶
Back
Close
Full Screen / Esc
Printer-friendly Version
Interactive Discussion

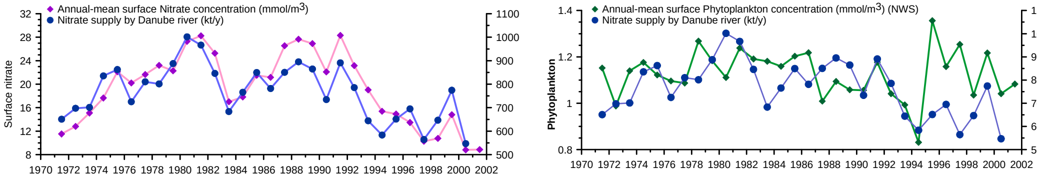

Fig. 13. Annual-mean surface nitrate (left) and phytoplankton (right) concentrations (derived from the modeling) on the northwestern shelf of the Black Sea and annual-mean nitrate supply by Danube river.

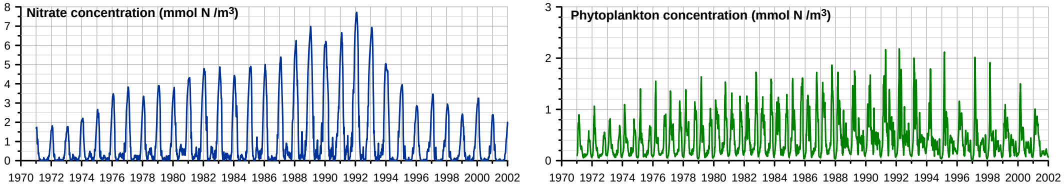

Fig. 14. Long-term evolution of the basin-averaged surface nitrate (left) and phytoplankton (right) concentrations in the deep part of the Black Sea (results of the modeling).

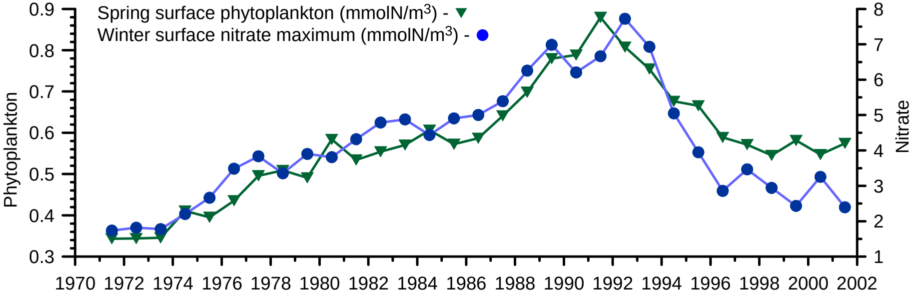

Fig. 15. Evolution of the basin-averaged winter surface nitrate maximum (spots) and spring-mean surface phytoplankton concentration (triangles) in the deep part of the Black Sea.

OSD
9, 2039–2080, 2012

Title Page
Abstract
Introduction
Conclusions
References
Tables
Figures
I◀
▶I
◀
▶
Back
Close
Full Screen / Esc
Printer-friendly Version
Interactive Discussion

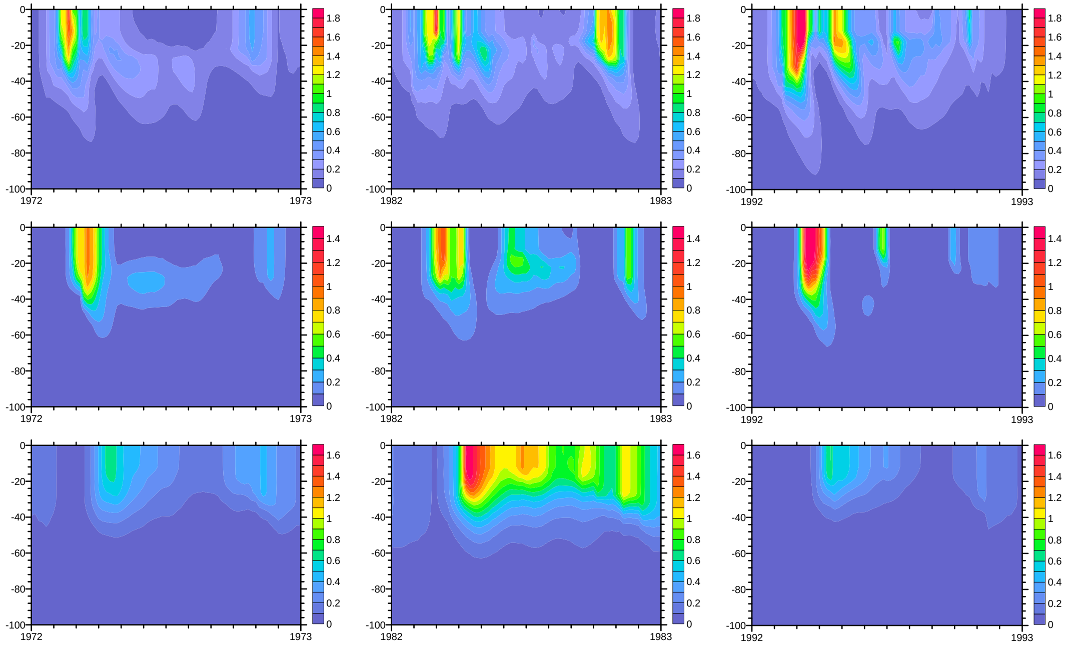

Fig. 16. Season evolution of the phytoplankton (upper row), zooplankton (middle row) and Aurelia aurita (lower row) (mmol N m^{-3}) in the central part of the Black Sea for three years: 1972 (left column), 1982 (central column) and 1992 (right column). (Results of the modeling.)

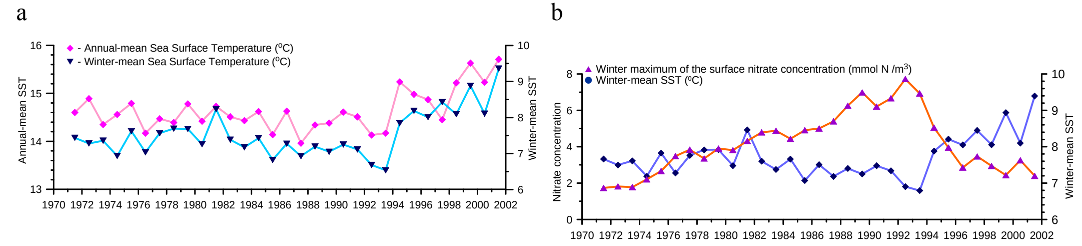

Fig. 17. Evolution of the basin-averaged annual (squares) and winter (spots) surface temperature; **(b)** winter nitrate maximum (triangles) and winter SST (spots) in the deep part of the Black Sea.

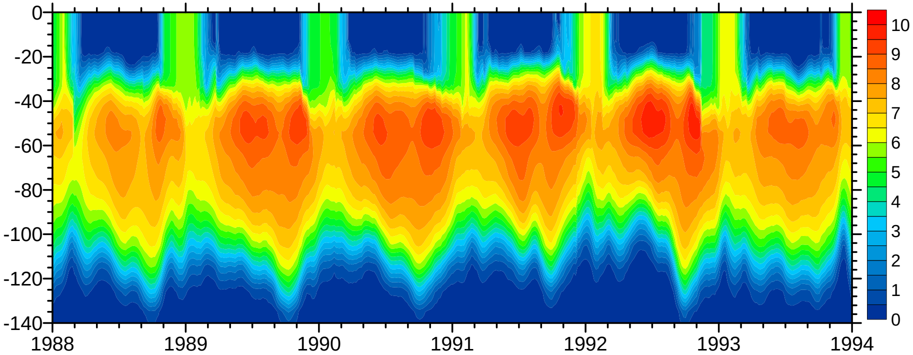

Fig. 18. Derived from the modeling six year evolution of the nitrate in the upper 140 m layer in the point in deep part of the Black Sea.

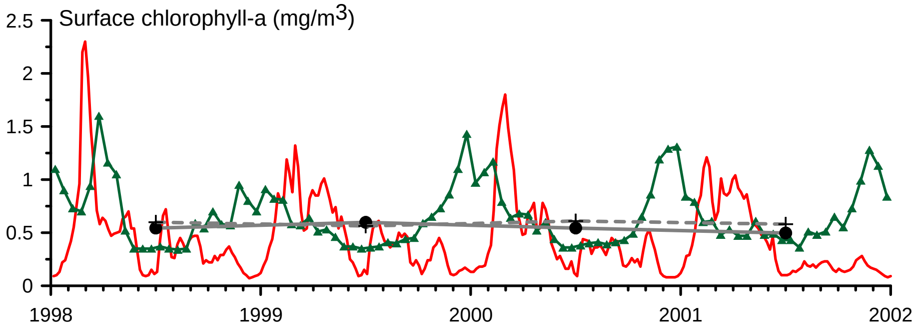

Fig. 19. Temporal evolution of the basin averaged surface chlorophyll concentration for the deep part of the basin derived from modeling (red line) and SeaWiFS data (green line). Spots and crosses denote year-mean values from modeling and SeaWiFS, respectively.

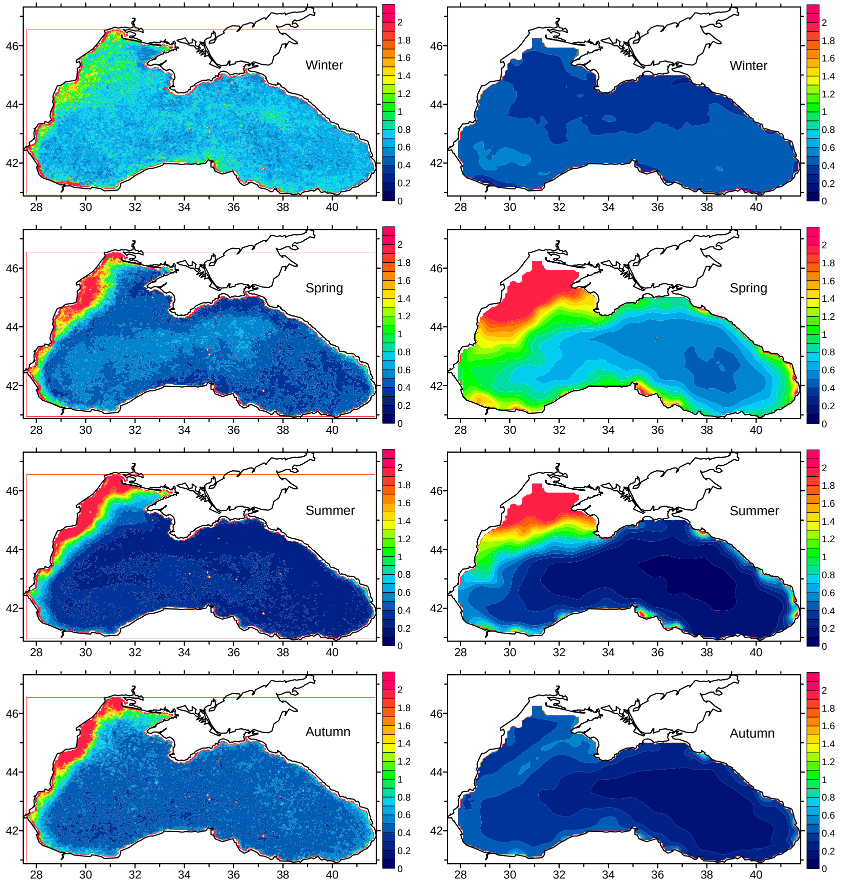

Fig. 20. Seasonal composite images of the surface chlorophyll, SeaWiFS data (left) and results of the modeling (right).

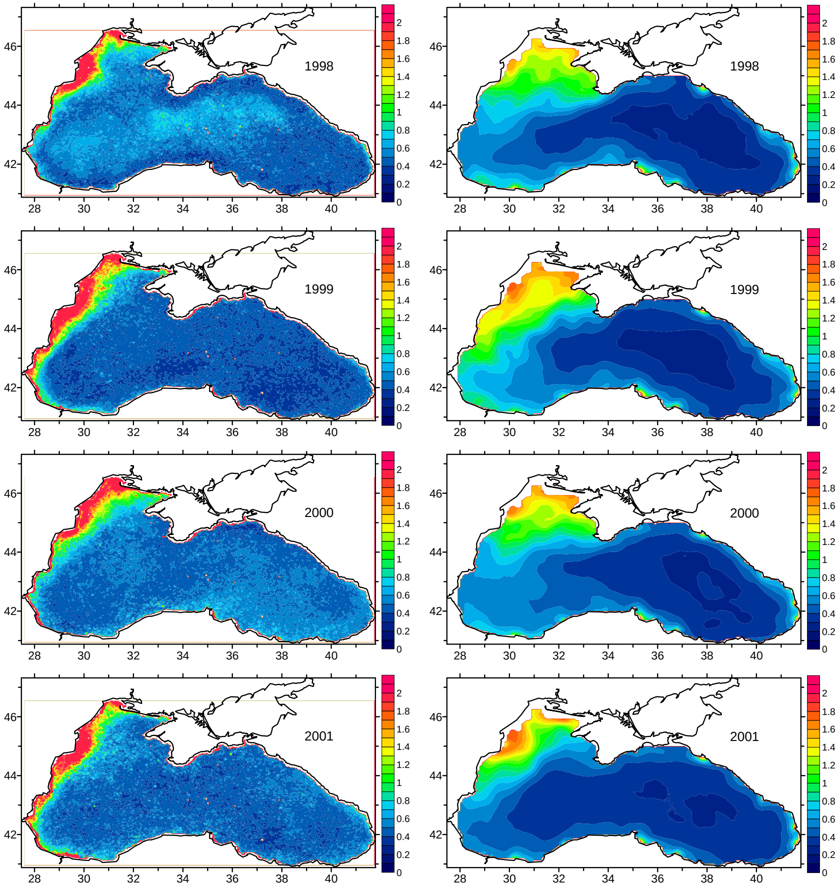

Fig. 21. Year-mean images of the surface chlorophyll, SeaWiFS data (left) and results of the modeling (right).

OSD

9, 2039–2080, 2012

Modeling long-term changes of the Black Sea ecosystem characteristics

V. L. Dorofeyev et al.

Title Page
Abstract
Introduction
Conclusions
References
Tables
Figures
I◀
▶I
◀
▶
Back
Close
Full Screen / Esc
Printer-friendly Version
Interactive Discussion